On the Performance and Accuracy of Enhanced Particle Finite Element Method (PFEM-2) in the Solution of Biomedical Benchmarks

Chien-Jung Huang, Facundo Del Pin, Iñaki Çaldichoury, Rodrigo R. Paz

LST LLC, an ANSYS company, Livermore, CA

Abstract

The numerical methods can be helpful on the R&D of medical devices to reduce the costly and lengthy process that clinical trials take for the US Food and Drug Administration (FDA) to approve a medical device. The FDA and academia are working together to create laboratory experiments that will help the industry gain confidence in numerical techniques as well as provide software developers with insights on the strengths and weaknesses of numerical software. In this study, three benchmarks proposed by the FDA are used to compare with experimental results with LS-DYNA® ICFD solver with a Finite Element Method (FEM) formulation and Enhanced Particle Finite Element Method (PFEM-2) formulation. In PFEM-2, on top of the finite element mesh, the advection effects are approximated in a Lagrangian way using particles carrying flow properties. This means no stabilization is needed for the Galerkin approximation of the advection term in the transport equations. The PFEM-2 enables analyzing a problem with a larger time step and is a big advantage in problems with flows at high Reynolds number. The first and second benchmark problems are the flows in a nozzle containing a gradual and a sudden change of diameter and flow in a simplified centrifugal blood pump with the goal of predicting hemolysis. The third benchmark studies the steady flow in a patient-averaged inferior Vena Cava.

Introduction

A key step in the development of medical devices is the testing phase. Regulatory agencies like the Food and Drug Administration require extensive laboratory testing and a long, tedious and expensive clinical trial process before a device is approved for clinical use. In an effort to optimize this process, the industry and the regulatory agencies are looking at numerical methods as an additional tool that could potentially reduce the time of product development, animal testing and cost. The first critical step is to increase the confidence, reliability and robustness of numerical techniques. The FDA is actively working on this subject by designing laboratory experiments that could be used to evaluate the solution accuracy provided by computational methods launching the Critical Path Initiative (CPI) [1] program. The aim of the program is to standardize the use of computational simulation on the design of the blood-contacting medical devices and analysis of the ratio of hemolysis in them. The goal of this project is to establish the guidelines for applying Computational Fluid Dynamics (CFD) techniques on the evaluation and the optimization of the medical devices. FDA has proposed two benchmark problems [2] for CFD verification and validation. The first benchmark problem is the study of the flow in a nozzle containing a gradual and sudden change of the diameter. The second benchmark problem is the analysis of the flow in a simplified centrifugal blood pump. For each benchmark problem, the experimental results [3,4,5] and the flow field predicted with numerical simulations [6,7,8,9] from different institutes are collected. The comparison between results obtained using different numerical models are made and analyzed [10,11]. The third benchmark problem presented involves the analysis of a steady flow in a patient-averaged inferior vena cava [12, 13]. Although there are many numerical results in this area only a few compare with flow measurements of experimental results. In particular, the study represents an anatomical model of the inferior vena cava (IVC) that includes the primary morphological features that influence the hemodynamics (iliac veins, infrarenal curvature, and non-circular vessel cross-section).

In this study, these three benchmark problems are presented and the experimental results are contrasted with numerical results using a Finite Element Method (FEM) formulation and the enhanced Particle Finite Element Method (PFEM-2) [14].

The main goal of this paper is to evaluate the performance of the PFEM-2 method implemented on the framework of LS-DYNA ICFD in the field of biomedical devices comparing the predictions with the experimental results. The PFEM-2 method is based on the idea that advection effects are approximated in a Lagrangian way using particles. Many numerical methods are based on these ideas [15,16,17,18,19] including the early version of PFEM [14]. The work of Idelsohn et. al. [20,21] introduced an strategy called X-IVS for integration of particle trajectory, while that employed a fixed mesh modifying. This provided PFEM-2 the advantage that larger time steps could be used [22] reducing the computational time in advection dominated problems and eliminating the traditional advection stabilization terms known to introduce additional numerical diffusion. By eliminating the advection term, a fractional step method provides a fully decoupled momentum equation among the three velocity components which saves storage and simplify the implementation. The method has also been successfully implemented for multi-phase flows [23,24,25,26], problems involving surface tension [27], fluid structure interaction [28] and thermal analysis [29]. The PFEM-2 has also been successfully tested in industrial applications that require long simulation times as documented in [30]. There are many applications in the biomedical field that could benefit from the capabilities of PFEM-2. In particular the applications that involve long real time simulations like drug delivery where a fluid component is injected in another fluid. In this case it is also important to keep track of the sharp interface at the drug advancing front.

In this work the implementation of PFEM-2 was performed in the commercial software LS-DYNA [31] which is a multi-physics solver for general non-linear dynamics. The module used for the implementation was ICFD solver which deals with incompressible fluid flows. The rest of this paper is organized as follows. In the first section the equations governing the flow of incompressible fluids will be presented together with boundary and initial conditions. In section two the PFEM-2 method will be introduced, and some implementation aspects will be discussed. In section three the time and space discretization of the equations of motion will be presented. In section four the benchmark problems will be introduced, and the experimental and numerical results will be presented.

Numerical Method

PFEM-2

In PFEM-2, the advection is tackled with Lagraingian particles. The rest of the governing equations are then solved separately with FEM formulation. These massless Lagraingian particles are added everywhere in the mesh, and they are not restricted to the mesh nodes. The advection is done by transporting the particles, which carry flow properties information including velocity and temperature, with local flow velocity.

In [20], Idelsohn et. al. presented an integration scheme called *eXplicit Integration following the Velocity Streamlines* (X-IVS) which is used to integrate the trajectory of particles in PFEM-2. Using this technique, the position of a particle q at time $t^{n+1}(x_q^{n+1})$ is computed using the velocity streamlines at t^n:

$$\begin{cases} x_q^{n+1} = x_q^n + \int_n^{n+1} u^n\left(x_q^\tau\right) d\tau \\ \hat{u}_q^{n+1} = u_q^n \end{cases} \tag{1}$$

where τ represents the time domain. The expression in Eq. (1) is explicit since it only depends on values from time step t^n while it maintains the high order approximation used for the velocity field. This expression is not an exact integration since the integral is evaluated following a pseudo-trajectory of the particles calculated with the velocity streamlines within each time step instead of following the true trajectory. Eq. (1) may be integrated analytically or using any standard time integration scheme like explicit Runge-Kutta or using sub-stepping. This new integration proposal provides an efficient strategy to employ time-steps which allow a Courant-Friedrich-Levy (CFL) number larger than one, where:

$$\mathrm{CFL} = \frac{|u|\,\Delta t}{\Delta x} \tag{2}$$

where Δt is the time step and Δx the mesh size. In summary, this means that each particle will be able to travel more than one element without compromising the stability of the method.

It is important to remark that the particles carry valuable information from all the states previous to their current location and preserving that information will have a big influence in the final accuracy of the method. That is why instead of interpolating the mesh velocity to the particle, the change of the mesh velocity should be applied. So in Eq. (1):

$$u_q^n = u_q^{n-1} + \sum_i N_i(x_q^n)(u_i^n - u_i^{n-1}) \tag{3}$$

being N_i the shape function of node i for the host element of particle q. In Fig. 1 the trajectory of a particle is computed using the X-IVS method, and it is compared to the trajectory of a first order integration scheme for $\mathrm{CFL} \gg 1$

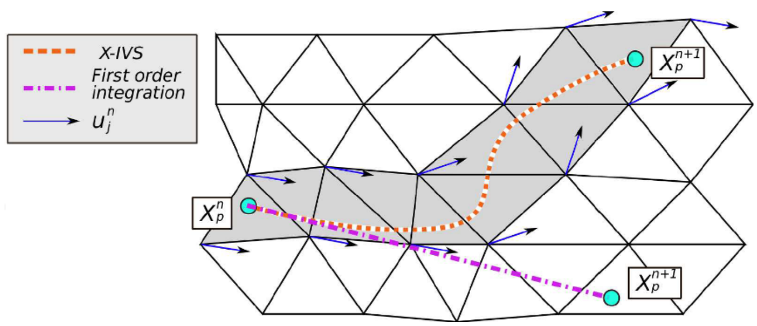

Fig. 1 Comparison of the trajectory of a particle moving from step n to n+1 for a given Δt using the X-IVS method and a first order integration method. The vectors represent the fluid velocity at step n.

Once the particles are moved to their new t^{n+1} position, the field ϕ that they transport (velocity, temperature, level set, etc.) needs to be mapped back to the mesh to perform the FEM analysis. Several approaches have been presented in [25]. In the current work the Global Least Squares Consistent (GLSC) methodology has been implemented and applied to our test cases. This approach solves a minimization problem where the approximation functions are the same linear shape functions used by the FEM discretization [32].

Another aspect of PFEM-2 which is more widely discussed in [33] is that of the particle inventory. Essentially it is the question of when, where and how to add or remove particles. In the present implementation particles are seeded into all the elements at initialization. All elements have the same amount of particles with randomly generated positions. In this work, all elements are seeded with twelve initial particles in 3D and nine in 2D. To control the total particle number, Gimenez et. al. [33] mentioned a particle removal approach (R-1) by removing two or more particles at almost the same location. In this study, if two or more particles are within a circle (2D) or sphere (3D) of radius $r = \delta h$, where h is the size of element, these particles will be replaced by a new particle which its particle properties are averaged from the removed ones. The value of δ is chosen to be a constant 0.2 so that the total particle number will be within acceptable range without deteriorating the result. An example of flow past a 2D cylinder shows the difference with particle removal treatment. In Fig. 2, it illustrates that initially all elements have the same number of particles. As the flow evolves, particles agglomerate increasing the overall amount of particles in the domain without any particle removal approach, compared with much less particle with particle removed. The highly uneven distribution of the particle without any removal can also deteriorate the scalability in parallel computing. This will be discussed in the next section. Fig. 3 depicts the evolution of particle number. The number of particles reaches to around 280 thousand without any particle removal and maintains around 57 thousand particles with particle removal treatment. The discrepancy on drag force generated on cylinder is only 0.64% between with and without particle removal.

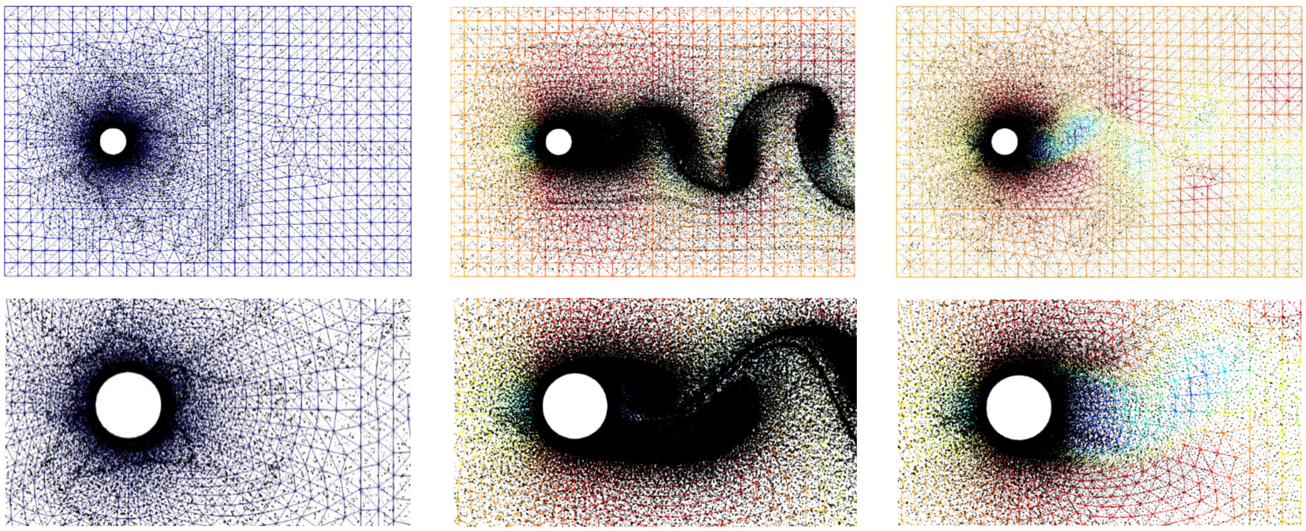

Fig. 2 Particle distribution in the domain and a closer view near the cylinder at initial (left) configuration, at the end time with no removal strategy (middle), and with removal strategy (right).

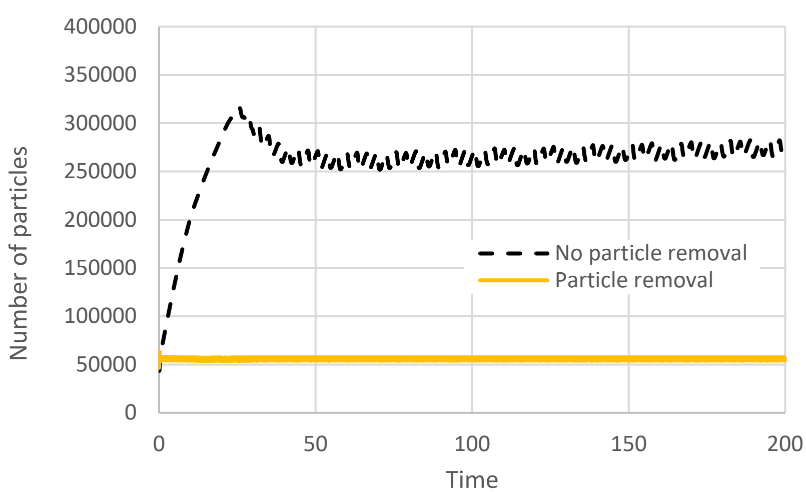

Fig. 3 Number of particles without and with the present removal strategy.

In summary, in one-time step, firstly the particles are moved with X-IVS scheme. After mapping the updated velocity field to the mesh, the FEM formulation is solved on the mesh. It is followed by correction of particle velocities by interpolating the velocity change on the mesh back to particles. Lastly, the particle inventory management is performed by adding or removing particles.

Parallel Implementation

The parallel implementation for PFEM-2 follows the guidelines presented by Gimenez et. al. in [22] for the case of distributed memory architectures. The challenges of serial implementations are well described by Gimenez et. al. and basically involves the extra amount of memory needed for the particle data structure. Due to the explicit scheme, the parallel implementation needs to take care of local operations for each particle separately from the rest allowing for a relatively simple parallelization. The difficulty arises at the interface between processors where particles may travel several elements or processors before finding their final host element. This task requires an outer loop to communicate particles among processors. This loop will terminate when no more particles cross the interface between partitions. In Fig. 4 there is an illustration of how particles may move across processors. The thick black line depicts the partition. In the first case a particle lands in the same processor which involves no communication. In the second case a particle moves across a single interface and communication takes place. In the third place a particle may move across two or more processors in which case the outer loop will perform as many communications as necessary until no more particles cross a processor interface. The current approach is built “on top" of the parallel FEM implementation of LS-DYNA ICFD solver. Thus it inherits much of the data structures and methodologies where the partitions are created using the software METIS [34, 35].

To exemplify scalability a 3D problem of the flow past a cylinder is used. It has a relatively small number of elements (of about 200 thousand) compared to the element numbers used in the application examples.
In Fig. 5 illustrates the strong scalability with different inventory strategy of PFEM-2 for distributed memory parallelization. There show three different inventory strategies of particle removal approaches. In the first case, no particle is removed from the model except for those that leave the domain and particles are added in elements with less than 12 particles. The final number reaches about 30 million particles. Since there are no load balancing particles, particles accumulate in certain elements are expected to degrade the scalability, which is what is observed in Fig. 5. In the second case, the number of particles is kept constant at each element regardless of the accuracy of the result. The total number of particles in this case is around 5.7 million. In the last case, the particle removal strategy is performed as mentioned in the previous section, and total number of particles reaches to around 5.5 million. The scalability for the second and the third cases compares well with that of [22].

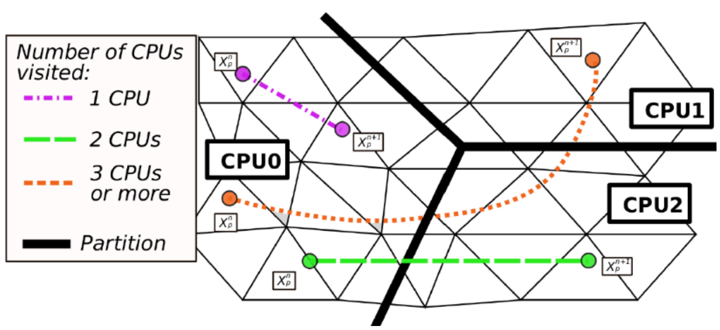

Fig. 4 Different ways that particles may move across processor interfaces.

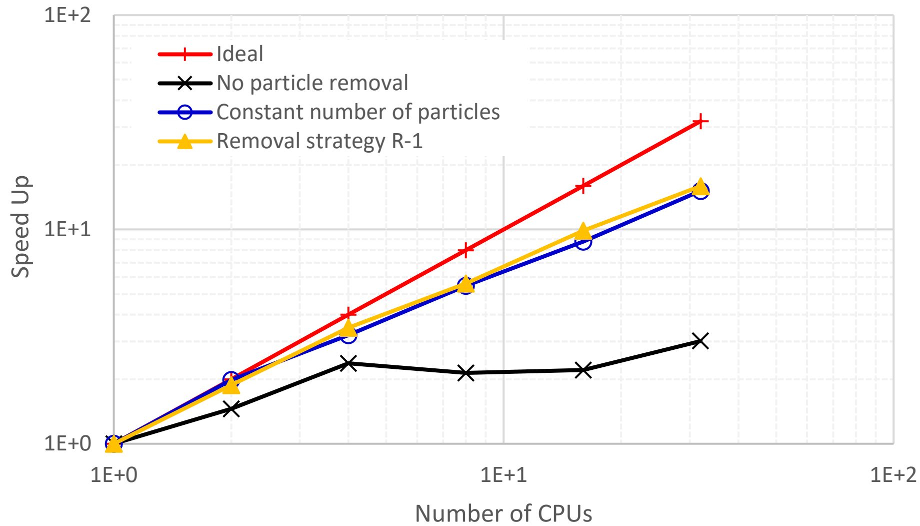

Fig. 5 Scalability analysis with different particle removal approaches.

Results

The flow fields in idealized blood nozzle, blood pump proposed by FDA and the IVC are simulated with LS-DYNA ICFD FEM and PFEM-2 solvers, and are compared with experimental results [3,4,5,12]. The fluids in all these simulations are assumed to be blood analog Newtonian fluid. For the nozzle and pump flows, the fluid density and viscosity are ρ= 1035 kg/m^3 and μ =3.5×10^{-3} N-s/m^2. As to the IVC flows, numerical simulations of resting and exercising conditions are conducted. The density and viscosity are ρ=1817 kg/m^3, μ=5.83×10^{-3} N-s/m^2 for resting condition and μ=5.49×10^{-3} N-s/m^2 for exercising condition.

Flow in the blood nozzle

The three-dimensional simplified nozzle proposed by FDA consists of four parts representing characteristics of some blood-conveying medical devices. There are inlet and outlet tubes with diameter 0.012 m, as well as a cone-shaped converging tube connecting the inlet tube with the nozzle throat with diameter 0.004 m as shown in Fig. 6. The flow experiences a gradual contraction of area from the inlet tube to the throat, then a sudden expansion of area right after the throat to the outlet. The z coordinate along the axial direction has origin at the exit of the nozzle throat. The flow at Reynolds number 3500 with flowrate 3.64×10^{-5} m^3/s corresponding to turbulent flow regime is analyzed, where the Reynolds number is defined with the flow rate and the diameter at the throat.

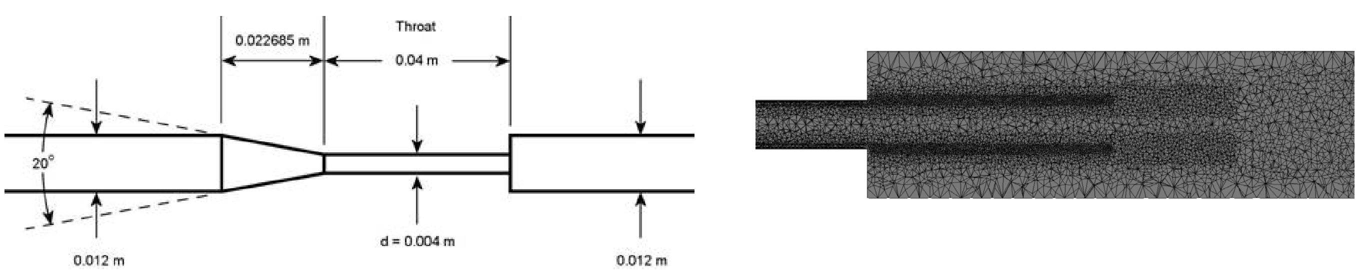

Fig. 6 The dimension of the blood nozzle (left) and the mesh near the outlet of the nozzle throat (right). The flow direction is left to right.

The numerical domain of the nozzle starts from z = -0.18 m to z = 0.18 m. A uniformly distributed velocity profile is imposed at the inlet while the pressure is set to be constant at outlet. To take care of the turbulence regime, the Large Eddy Simulation (LES) Smagorinsky model is used, and the Smagorinsky coefficient is set to be 0.1 (empirically derived for flows in pipes). The turbulence intensity at the inlet is set to be 5% (see Smirnov's turbulence synthesis method [36]). The simulation domain is decomposed into 1.13 million tetrahedral elements. The mesh is refined near the exit of the throat with minimum mesh size 0.1 mm. Simulations with two CFL numbers 1 and 10 are conducted examine the influence of the time step size with these two methods.

The obtained distributions of the instantaneous velocity magnitude in the nozzle after reaching steady state are shown in Fig. 7. It can be observed that the sudden expansion at the exit of the throat leads to the formation of a jet. In turbulent regime, jet breakdown occurs so that the center velocity of the jet has a sudden decrease. Most of the obtained results show the breakdown of the jet, but with different breakdown locations. Fig. 8 shows the time-averaged velocity along the center line of the nozzle, where the origin of the axial z coordinate is at the exit of the throat. The breakdown locations predicted by FEM and PFEM-2 with CFL=1 both have a good agreement with experiments [7]. When the time step size increases, the results using PFEM-2 are not affected much. This implies PFEM-2's solution is within the statistical dispersion of the method. A further statistical analysis (which is outside of the scope of this paper) could help quantify the spread of the solution when the time steps increase. On the other hand, for the results using FEM, the estimated breakdown locations of the jet are affected more when the CFL number is larger than 1.

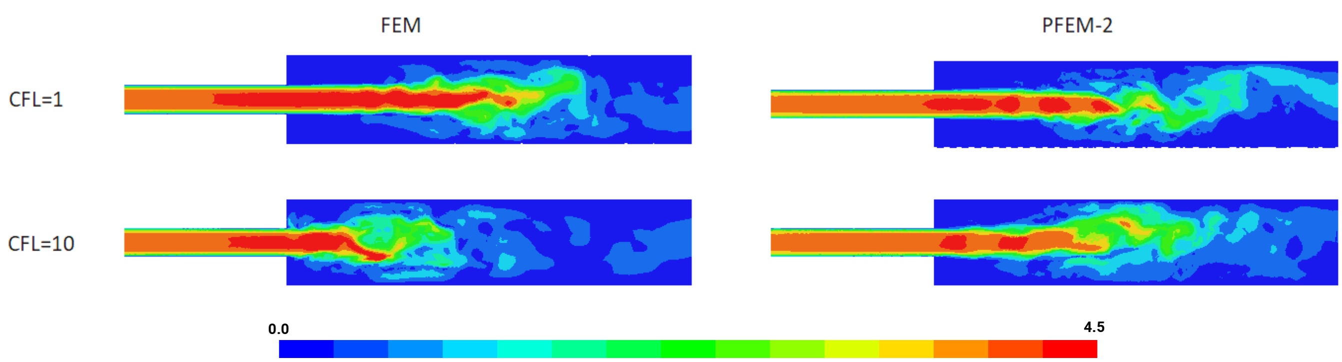

Fig. 7 Instantaneous velocity fields in blood nozzle using FEM and PFEM-2 solvers with different CFL numbers.

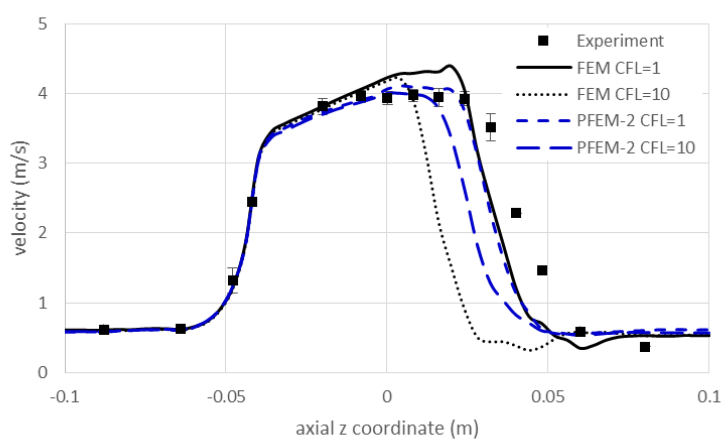

Fig. 8 The time-averaged velocity profiles in the nozzle along the center line.

Flow in the blood pump

The geometry of the FDA proposed simplified centrifugal pump is shown in the Fig. 9. The flow enters the chamber through a curved tube with diameter 12 mm. The diameter of the inner chamber of the housing is 60 mm and the thickness is 9 mm. The rotor inside the chamber has a diameter of 52 mm and 4 mm thick, along with four 3 mm thick straight blades. The chamber is connected with a throat at its outlet, followed by a diffuser to the outlet tube with diameter 12 mm. The pump flow with flowrate Q = 6 L/min and rotational speed 3500 RPM is analyzed.

For the simulation set up, the velocity distribution is prescribed at the inlet, where the velocity profiles are obtained from the experimental measurements using PIV [1]. The pressure at the outlet is set to be constant. Since the goal is to predict the flow field after reaching steady state, instead of letting the rotor rotate during simulation, the non-inertial reference frame is applied on the fluid around the rotor. This is because the flow around the rotor at steady state can be analogue to flow experiencing constant angular velocity. Using non-inertial reference frame approximation avoids mesh distortion and frequent remeshing due to rotation. The LES Wall-Adapting Local Eddy-viscosity (WALE) [37] turbulence model is employed. The simulation domain is decomposed into around 1 million tetrahedral elements (Fig. 9). The minimum mesh size is 0.5 mm on the rotor blades and 0.3 mm at the outlet of the chamber to the diffuser. The mesh is locally refined around the throat as shown in Fig. 9. The simulation result is obtained after 20 rotations when the pump flow already reaches steady state. The time step size is around 10^{-5} s in FEM and PFEM-2 simulations at steady state so that the CFL number is less or equal than 1.

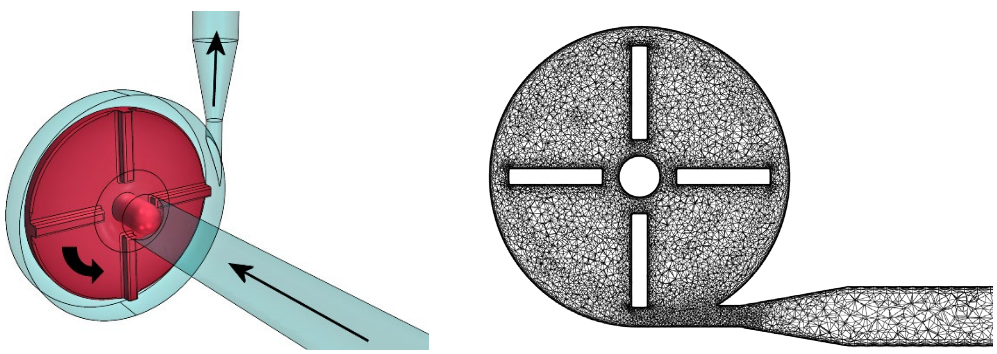

Fig. 9 Blood pump geometry and the flow direction in the pump (left). The mesh configuration used in the pump flow simulations on the plane coinciding with the mid-axis plane of the outlet diffuser (right)

Table 1 shows the pressure difference across the pump obtained by the experiment and the. Using FEM the discrepancy with experiment is only 3.6%. On the other hand, PFEM-2 predicts a lower pressure difference with 18.7% discrepancy compared to the experiment. From the distribution of the velocity and pressure fields in the chamber (Fig. 10 and Fig. 11), the results by PFEM-2 and FEM are qualitatively in accordance with each other. Fig. 12 depicts the comparison of the velocity profile in the pump chamber and diffuser compared with several experimental measurements [11]. The velocity profile between blades by FEM and PFEM-2 are both in accordance with experiments. In the outlet diffuser, FEM and PFEM-2 predict the detached jet leaning more toward the outer wall and the velocity magnitude appears to be larger than experiments. The phenomenon may be due to the usage of the non-inertial reference frame approximation since similar velocity distribution in the diffuser can also be observed in most of the other numerical results that use non-inertial reference frame [11].

Table 1 The pressure difference across the pump.

	Pressure (mmHg)
Experiment [11]	272.38
FEM	282.40
PFEM-2	221.27

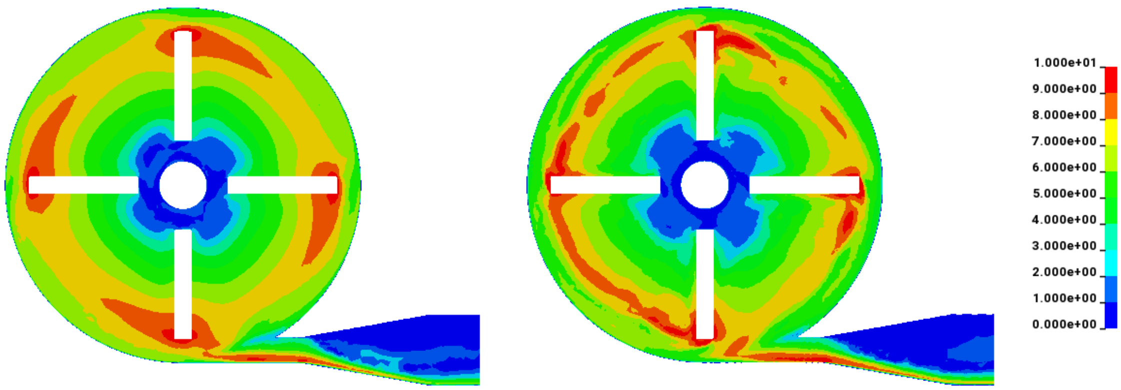

Fig. 10 Time-averaged velocity field after 20 rotations in blood pump with FEM (left) and PFEM-2 (right).

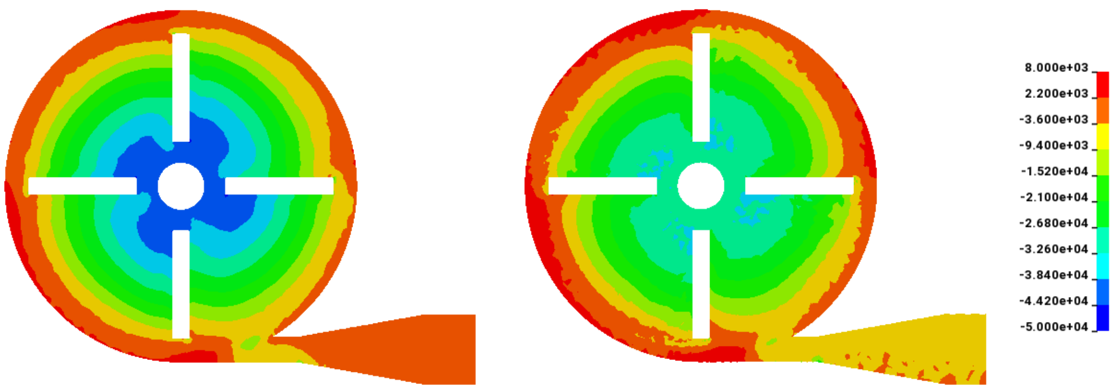

Fig. 11 Time-averaged pressure field after 20 rotations in blood pump with FEM (left) and PFEM-2 (right).

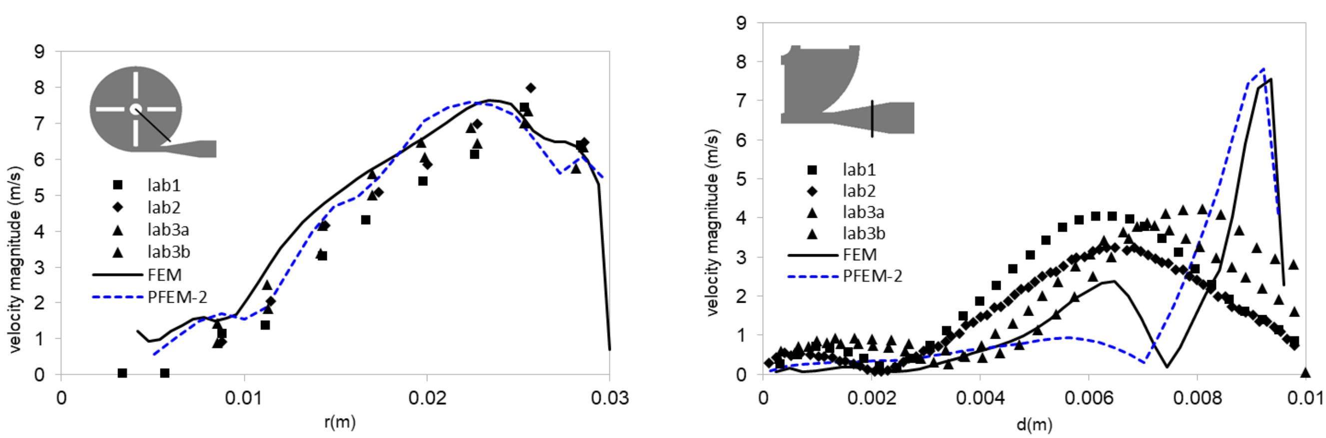

Fig. 12 The magnitude of the two-dimensional velocity on the plane coinciding with the mid-axis plane of the outlet diffuser with experiments and simulations. Left: velocity profile between two blades, where r refers to the distance to rotor center. Right: velocity profile across the outlet diffuser, where d refers to distance to the inner wall.

Flow in idealized Vena Cava

In present study, the geometry of the IVC system consists of two iliac veins merging to one infrarenal IVC as shown in Fig. 13. This patient averaged IVC geometry is proposed by [12] from the CT data of 10 patients. The flows enter from the two iliac veins and merge after entering the infrarenal IVC, which has a hydraulic diameter of about 28 mm. The simulations of the flow in the IVC are conducted according to the parameters provided in [13].

The simulations of two flowrates are performed corresponding to the resting and exercising conditions, which are Q = 0.5 L/min and 3 L/min into two iliac veins respectively. The corresponding Reynolds numbers for resting and exercising conditions are 236 and 1505. The flow is considered to be laminar in the IVC. A parabolic velocity profile is prescribed at the inlet of the two iliac veins, and a constant pressure boundary condition is imposed at the outlet of the infrarenal IVC. The domain is decomposed into 2.04 million and 4.7 million tetrahedral meshes for resting and exercising conditions, where the minimum mesh size in these two cases are 1.4 mm and 1.0 mm. These meshes sizes are chosen after grid convergence test [32].

The velocity fields predicted by FEM and PFEM-2 methods are compared quantitatively with PIV experimental results obtained by [12] on a selected sagittal plane and a coronal plane after the two veins merges as illustrated in Fig. 14 at two flow conditions. The FEM and PFEM-2 solvers use the same mesh under the same flow conditions. The experimental and simulation results of the in-plane 2D velocity magnitudes in the sagittal and coronal planes at resting and exercising conditions are shown in Fig. 15 and Fig. 16. The figures show that the results by FEM and PFEM-2 solvers both match qualitatively with the PIV results. Note that the imperfections observed in the form of holes originate in the mesh used for the PIV data which is the one used to map the numerical results for the comparison.

To do quantitative comparison with experiments, the numerically obtained nodal velocities are firstly sampled on to the PIV data points. The magnitude of 2D plane velocity is then calculated on each data points. The global relative error, E, can be obtained by averaging the relative error between numerical and experimental result on all points. Table 2 and Table 3 shows the global relative error at different flow conditions with FEM, PFEM-2 solvers as well as the numerical analysis reported in [13]. The global relative error is around 5 to 6% at resting condition and 6 to 11% at exercising condition. The obtained numerical results have a good agreement with the experimental data. For both conditions, the FEM and PFEM-2 results have similar amount of global relative error with [13]. It is worth noting that the mesh sizes used here (1.4 mm for resting and 1 mm for exercising conditions) are coarser than the mesh size (0.276 mm) used in [13]. Also, the PFEM-2 has nearly the same error compared with FEM at resting condition, and even less error in the coronal plane at exercising condition.

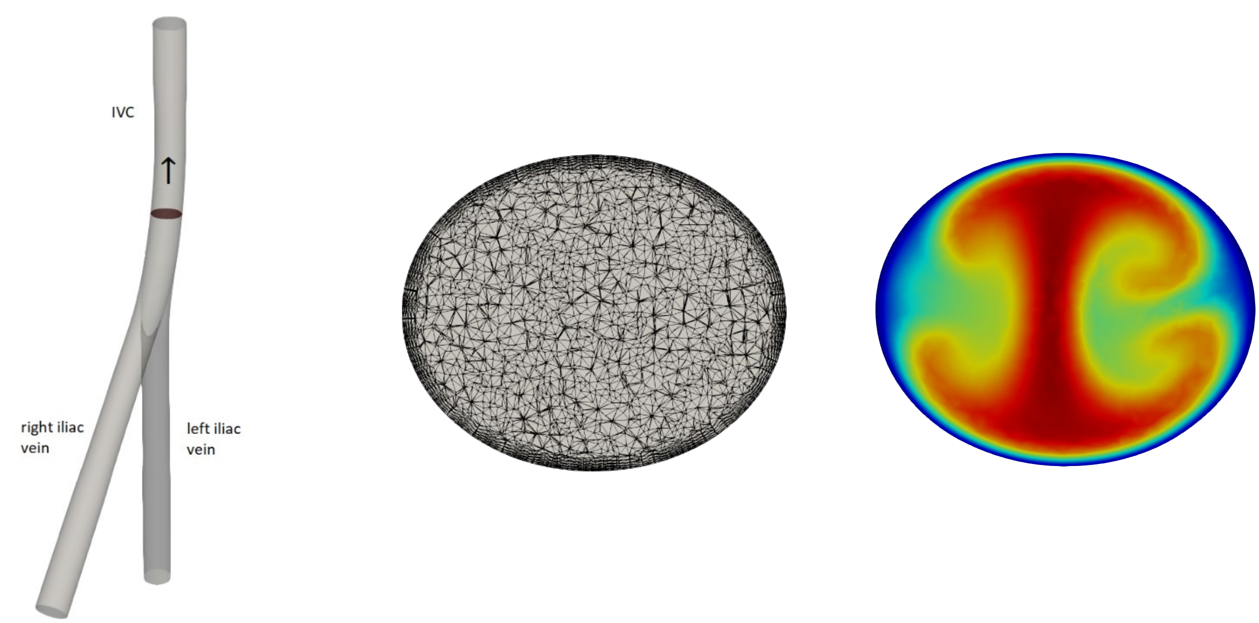

Fig. 13 The geometry of the IVC (left). The mesh (middle) and the obtained velocity magnitude (right) at exercise condition in the cross-sectional plane located at 10 cm after veins merging.

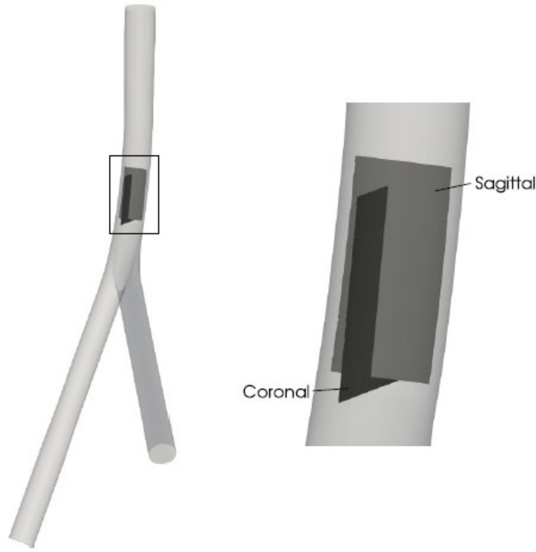

Fig. 14 The sagittal and coronal planes where the velocity field is measured in experiment [12].

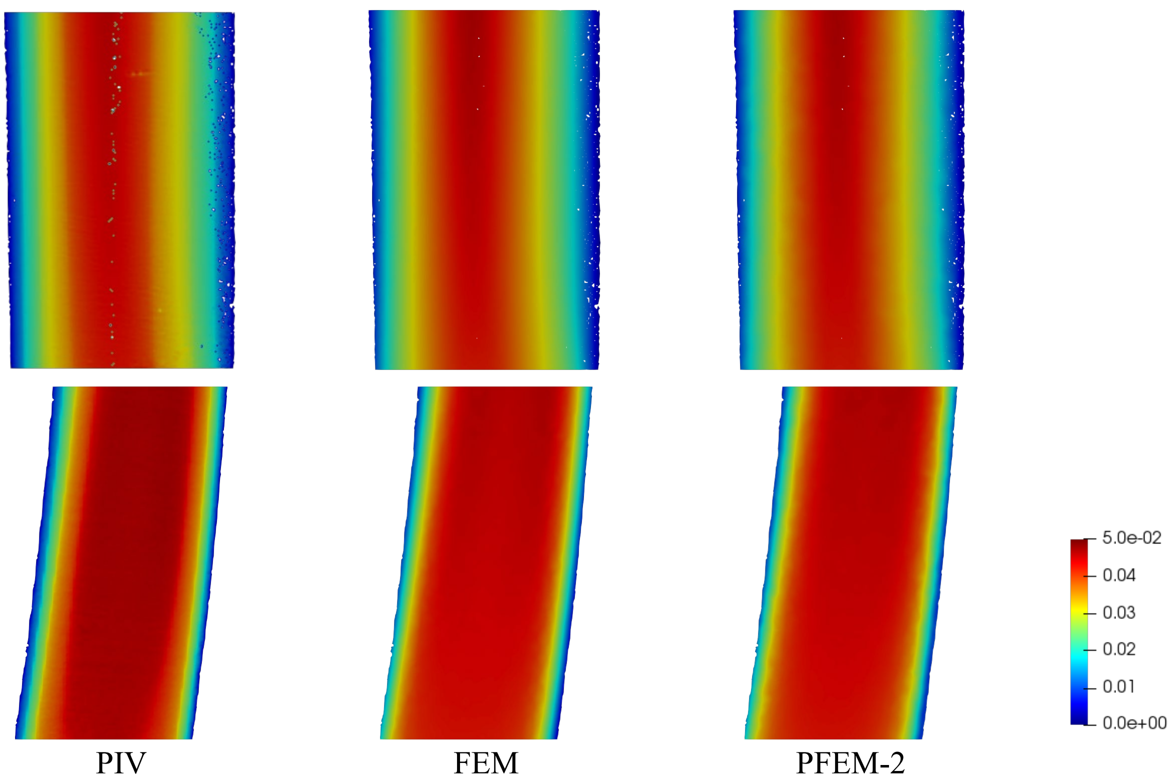

Fig. 15 The in-plane 2D velocity magnitude in coronal (top) and sagittal (bottom) planes of PIV, FEM and PFEM-2 results at resting condition.

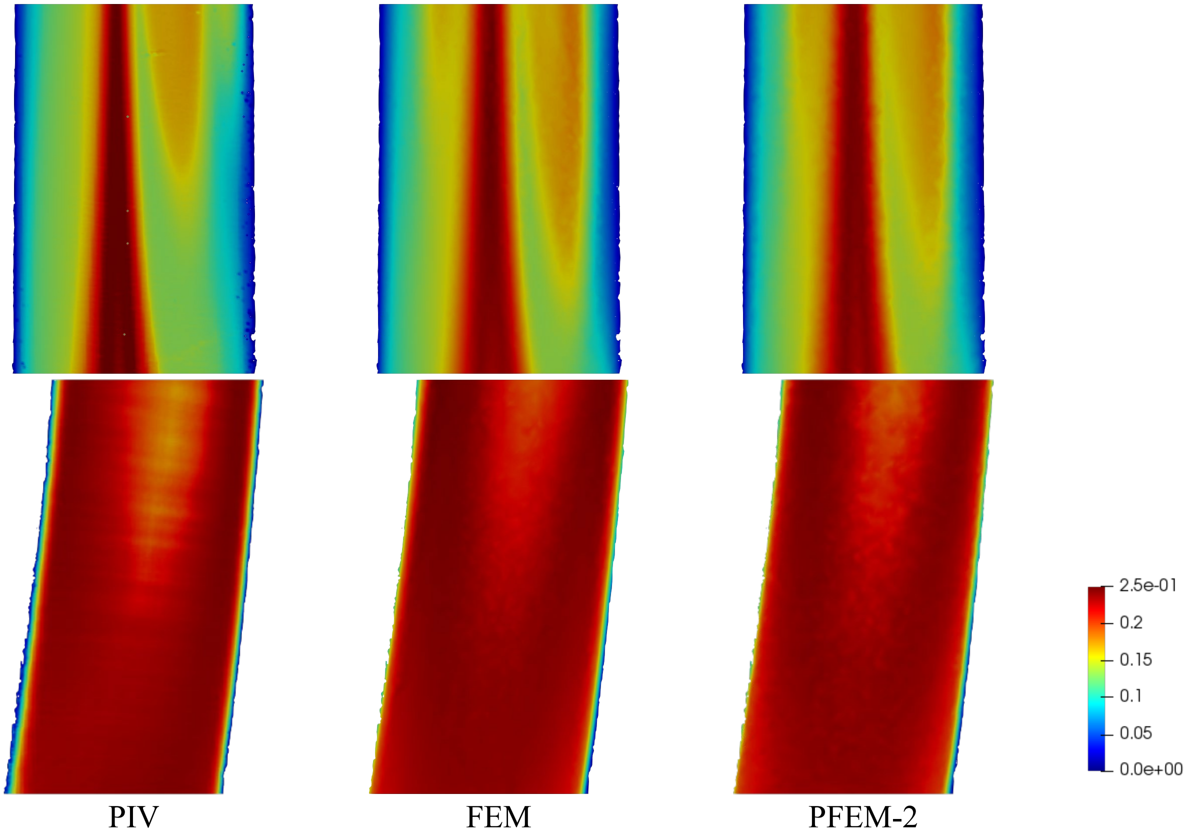

Fig. 16 The in-plane 2D velocity magnitude in coronal (top) and sagittal (bottom) planes of PIV, FEM and PFEM-2 results at resting condition.

Table 2 The global relative error at rest condition.

	Coronal	Sagittal
Craven et.al.[13]	3.07	6.77
FEM	4.83	6.62
PFEM-2	4.79	6.65

Table 3 The global relative error at exercise condition.

	Coronal	Sagittal
Craven et. al [13]	10.98	5.56
FEM	11.28	5.93
PFEM-2	10.44	6.10

Conclusion

In the present study, the numerical scheme of PFEM-2 implemented on LS-DYNA ICFD framework was applied on biomedical problems. In PFEM-2, the advection term is dealt with separately by transporting massless Lagrangian particles. These Lagrangian particles move with local velocities following the X-IVS integration scheme. The rest of the governing equations were tackled with a fractional step method on a fixed finite element mesh. The advantage of PFEM-2 is that it allows the use of a larger time step size allowing a CFL number much larger than 1 without compromising the stability and accuracy. The particle removal strategy was applied to control total number of particles without deteriorating the accuracy. The parallel implementation was introduced to tackle with particles moving across multi-processors during the advection stage, and the scalability performance with different inventory strategies was presented.

The PFEM-2 was applied to benchmark problems in the biomedical field for a FDA blood nozzle and pump, as well as IVC flows. The results of PFEM-2 are compared with results obtained from classical FEM formulation and experimental measurements in previous studies. Firstly, the nozzle flow at Re = 3500 is simulated with different time step sizes. The resultant jet breakdown locations using FEM differ largely with CFL numbers larger than 1, while PFEM-2's results differ less preserving a good agreement with experiments even with CFL = 10. Secondly the flow in a simplified blood bump geometry was studied, numerical simulations were performed under the non-inertial frame approximation. The pressure difference estimated by FEM has a 3.6% of discrepancies with the experimental value while PFEM-2 predicted a lower pressure difference across the pump with an error of 18.7%. Although the pressure differential error is higher for PFEM-2, the velocity profiles at different cross sections of the pump are in good agreement with the ones from FEM. Lastly, the flow in a patient-averaged IVC geometry was analyzed at resting and exercising conditions. The quantitative error of the in-plane velocity on selected sagittal and coronal planes were computed with different numerical approaches. Both FEM and PFEM-2 obtained nearly the same error at resting condition while PFEM-2 obtained a better result on a coronal plane at exercising condition.

As a final conclusion, it is evident from the results that PFEM-2 shows less sensitivity to time step size when compared to the FEM formulation presented in this paper. The advantage of PFEM-2 becomes more evident in problems of higher Reynolds number.

References

1. FDA Critical Path Initiative (CPI) https://www.fda.gov/scienceresearch/specialtopics/criticalpathinitiative/default.htm
2. FDA's "Critical Path" Computational Fluid Dynamics (CFD)/Blood Damage Project: Computational Round Robin problems https://nciphub.org/wiki/FDA_CFD
3. Hariharan P, Giarra M, Reddy V, Day SW, Manning KB,Deutsch S, Stewart SF, Myers MR, Berman MR, Burgreen GW, Paterson EG (2011). Multilaboratory particle image velocimetry analysis of the FDA benchmark nozzle model to support validation of computational fluid dynamics simulations. Journal of Biomechanical Engineering, 133(4):041002-1.
4. Herbertson LH, Olia SE, Daly A, Noatch CP, Smith WA, Kameneva MV, Malinauskas RA (2015). Multilaboratory Study of Flow-Induced Hemolysis Using the FDA Benchmark Nozzle Model. Artificial Organs, 39(3):237-248.
5. Giarra MN (2009). Shear Stress Distribution and Hemolysis Measurements in a Centrifugal Blood Pump. Master Thesis, Rochester Institute of Technology. Rochester, New York.
6. Zmijanovic V, Mendez S, Moureau V, Nicoud F (2017). About the numerical robustness of biomedical benchmark cases: Interlaboratory FDA's idealized medical device. International Journal for Numerical Methods in Biomedical Engineering, 33(1):e02789.
7. Hariharan P, D'Souza GA, Horner M, Morrison TM, Malinauskas RA, Myers MR (2017). Use of the FDA nozzle model to illustrate validation techniques in computational fluid dynamics (CFD) simulations. PloS One, 12(6):e0178749.
8. Nassau CJ, Wray TJ, Agarwal RK (2015). Computational Fluid Dynamic Analysis of a Blood Pump: An FDA Critical Path Initiative. In ASME/JSME/KSME 2015 Joint Fluids Engineering Conference (pp. V002T26A002-V002T26A002). American Society of Mechanical Engineers.
9. Heck ML, Yen A, Snyder TA, O'Rear EA, Papavassiliou DV (2017). Flow-Field Simulations and Hemolysis Estimates for the Food and Drug Administration Critical Path Initiative Centrifugal Blood Pump. Artificial Organs, 41(10):E129-E140. doi: 10.1111/aor.12837.
10. Stewart SF, Paterson EG, Burgreen GW, Hariharan P, Giarra M, Reddy V, Stewart SF, Paterson EG, Burgreen GW, Hariharan P, Giarra M, Reddy V, Day SW, Manning KB, Deutsch S, Bermand, MRm, Myers MR (2012). Assessment of CFD performance in simulations of an idealized medical device: results of FDA's first computational interlaboratory study. Cardiovascular Engineering and Technology, 3(2):139-160.
11. Malinauskas RA, Hariharan P, Day SW, Herbertson LH, Buesen M, Steinseifer U, Aycock KI, Good BC, Deutsch S, Manning KB, Craven BA (2017). FDA benchmark medical device flow models for CFD validation. ASAIO Journal, 63(2):150-160.
12. Gallagher MB, Aycock KI, Craven BA, Manning KB (2018). Steady flow in a patient-averaged inferior vena cava-part I: particle image velocimetry measurements at rest and exercise conditions. Cardiovascular Engineering and Technology, 9(4):641-653.
13. Craven BA, Aycock KI, Manning KB (2018). Steady Flow in a Patient-Averaged Inferior Vena Cava-Part II: Computational Fluid Dynamics Verification and Validation. Cardiovascular Engineering and Technology, 9(4):654-673.

14. Idelsohn SR, Oñate E, Del Pin F (2004). The particle finite element method a powerful tool to solve incompressible flows with free surfaces and breaking waves. International Journal for Numerical Methods in Engineering, 61:964-989.
15. Monaghan JJ (1988). An introduction to SPH. Computer Physics Communications, 48:89-96.
16. Harlow FH (1955). A machine calculation method for hydrodynamic problems. Los Alamos Scientific Laboratory Report LAMS-1956.
17. Harlow FH, Welch J (1965). Numerical calculation of time dependent viscous incompressible flow of fluid with free surface. Physics of Fluids, 8(12):2182-2189.
18. Wieckowsky Z (2004). The material point method in large strain engineering problems. Computer Methods in Applied Mechanics and Engineering, 193(39):4417-4438.
19. Koshizuka S, Oka Y (1996). Moving particle semi-implicit method for fragmentation of incompressible fluid. Nuclear Science and Engineering, 123:421-434.
20. Idelsohn SR, Nigro NM, Limache A, Oñate E (2012). Large time-step explicit integration method for solving problems with dominant convection. Computer Methods in Applied Mechanics and Engineering 217-220:168-185.
21. Idelsohn SR, Nigro NM, Gimenez JM, Rossi R, Marti J (2013). A fast and accurate method to solve the incompressible Navier{Stokes equations. Engineering Computations, 30(2):197-222.
22. Gimenez JM, Nigro NM, Idelsohn SR (2014). Evaluating the performance of the particle finite element method in parallel architectures. Computational Particle Mechanics, 1(1):103-116.
23. Idelsohn SR, Marti J, Becker P, Oñate E (2014). Analysis of multifluid flows with large time steps using the particle finite element method. International Journal for Numerical Methods in Fluids, 75(9):621-644.
24. Gimenez JM, Gonzlez LM (2015). An extended validation of the last generation of particle finite element method for free surface flows. Journal of Computational Physics, 284:186{205.
25. Gimenez JM (2015). Enlarging time-steps for solving one and two phase flows using the particle finite element method. Ph.D. Thesis, Universidad Nacional del Litoral, Santa Fe, Argentina.
26. Salazar F, San-Mauro J, Celigueta MA, Oñate E (2017). Air demand estimation in bottom outlets with the particle finite element method. Computational Particle Mechanics, 4:345-356. https://doi.org/10.1007/s40571-016-0117-4.
27. Gimenez JM, Nigro N, Oñate E, Idelsohn S (2016). Surface tension problems solved with the particle finite element method using large time-steps. Computers and Fluids, 141:90-104.
28. Becker P, Idelsohn SR, Oñate E (2014). A unified monolithic approach for multi-fluid flows and fluid-structure interaction using the particle finite element method with fixed mesh. Computational Mechanics, 55(6):1091-1104.
29. Marti J, Ryzhakov P (2019). An explicit/implicit Runge-Kutta-based PFEM model for the simulation of thermally coupled incompressible flows. Computational Particle Mechanics, In press. https://doi.org/10.1007/s40571-019-00229-0.
30. Gimenez JM, Ramajo DE, Marquez-Damian S, Nigro N, Idelsohn S (2017). An assessment of the potential of PFEM-2 for solving long real-time industrial applications. Computational Particle Mechanics, 4:251-267.https://doi.org/10.1007/s40571-016-0135-2.
31. LS-DYNA Manual. http://www.lstc.com/download/manuals.
32. Del Pin, F., Huang, C. J., Çaldichoury, I., & Paz, R. R. (2020). On the performance and accuracy of PFEM-2 in the solution of biomedical benchmarks. *Computational Particle Mechanics*, *7*(1), 121-138.
33. Gimenez JM, Nigro NM, Idelsohn SR (2012). Improvements to solve diffusion-dominant problems with PFEM-2. Mecanica Computacional, vol. XXXI:137-155.
34. Karypis G, Kumar V. METIS, a Software Package for Partitioning Unstructured Graphs and Computing Fill-Reduced Orderings of Sparse Matrices.
35. Karypis G, Kumar V (1998). A fast and high quality multilevel scheme for partitioning irregular graphs. SIAM Journal on Scientiflc Computing, 20(1):359-392.
36. Smirnov A, Shi S, Celik I (2001). Random flow generation technique for large eddy simulations and particle-dynamics modeling. Journal of Fluids Engineering, 123(2):359-371.
37. Nicoud F, Ducros F (1999). Subgrid-Scale Stress Modelling Based on the Square of the Velocity Gradient Tensor Flow. Turbulence and Combustion, 62(3):183-200.